Inorganica Chimica Acta 556 (2023) 121612

Contents lists available at ScienceDirect

Inorganica Chimica Acta

journal homepage: www.elsevier.com/locate/ica

Exploring the range of applicability of anisotropic optical detection in axially coordinated supramolecular structures

F. Goto [a], A. Calloni [a,*], I. Majumdar [a], R. Yivlialin [a], C. Filoni [a], C. Hogan [b,c], M. Palummo [c], A. Orbelli Biroli [d], M. Finazzi [a], L. Duò [a], F. Ciccacci [a], G. Bussetti [a]

[a] Dipartimento di Fisica, Politecnico di Milano, Piazza Leonardo Da Vinci 32, 20133 Milano, Italy
[b] Istituto di Struttura della Materia, Consiglio Nazionale delle Ricerche (ISM-CNR), Via Fosso del Cavaliere 100, 00133 Roma, Italy
[c] Dipartimento di Fisica and INFN, Università di Roma "Tor Vergata", via della ricerca scientifica 1, 00133 Roma, Italy
[d] Dipartimento di Chimica, Università di Pavia, via Torquato Taramelli 12, 27100 Pavia, Italy

ARTICLE INFO

Keywords:
Supramolecular structure
Porphyrin
RAS
AFM
PES
IPES

ABSTRACT

Ensuring the highest accuracy in determining the molecular assembling and the preservation of the chemical and physical properties of the molecules during the growth of organic layers requires a real-time monitoring of film formation. In this respect, optical techniques are preferred since they result in minimum organic film damage. Among these techniques, Reflectance Anisotropy Spectroscopy (RAS) proved to be the one with the highest sensitivity due to the development of intrinsic anisotropies in the optical response of molecular films, where molecular packing is driven by Van der Waals interactions. Recently, we proposed an original strategy to enable the growth of organic films via molecular self-assembly through highly directional coordination bonds. Herein, we consider a straightforward supramolecular structure employing axial bonds, based on the 1:1 assembly of a Co^{II} porphyrin (CoTPP) and a linear ligand (DPNDI). This system is characterized by a rather isotropic structure that might, in principle, result in a weak RAS signal. Therefore, in the present work, we critically assess the range of applicability of such a spectroscopy. A number of other surface science techniques, including Low Energy Electron Diffraction (LEED), photoemission spectroscopies (PES and IPES) and Atomic Force Microscopy (AFM) is employed to fully characterize the axially coordinated molecular film.

1. Introduction

Organic molecules play a key role in many natural phenomena; in the last 30 years, however, they have found application also in a wide variety of hybrid and purely organic devices, ranging from electronic components like diodes and rectifiers to sensors and energy storage devices [1–7]. In these technological applications, a real time monitoring of the molecular layers' growth is mandatory to ensure the quality of the prepared organic–inorganic or organic-organic interfaces.

Film growth monitoring techniques based on the diffraction of a beam of electrons, conventionally used in semiconductor-based growth protocols, are not suitable for organic materials because of film damage upon the release of energy on the sample by the electronic probe [8,9]. Instead, optical probes have been devised for this purpose. Surface Differential Reflectivity (SDR) was proposed by Proehl *et al.* [10] and Reflectance Anisotropy Spectroscopy (RAS) by Martin *et al.* [11].

In RAS spectroscopy, the acquired signal is proportional to the difference in the reflectivity (ΔR) of linearly polarized light, impinging close to normal to the sample's surface, along two orthogonal directions (α and β):

$$\frac{\Delta R}{R} = 2\frac{R_\alpha(\omega) - R_\beta(\omega)}{R_\alpha(\omega) + R_\beta(\omega)}.$$

The difference signal is then normalized with respect to the mean signal (R). Despite the fact that RAS can measure only a relative anisotropy, the detected anisotropy signal can be as small as 0.1‰ of the overall reflected signal [12].

On single layer molecular films, the anisotropy signal arises from one, or a combination of the following possibilities: (i) an intrinsic molecular property, (ii) the packing of adjacent molecular units favouring, for instance, a tilting of the molecular axis with respect to the substrate, and (iii) an arrangement of the molecular domains showing a preferential alignment along a specific direction. In multilayer films driven by Van der Waals interactions, an additional anisotropy signal

* Corresponding author.
E-mail address: alberto.calloni@polimi.it (A. Calloni).

https://doi.org/10.1016/j.ica.2023.121612
Received 15 April 2023; Received in revised form 29 May 2023; Accepted 31 May 2023
Available online 3 June 2023

can arise from the formation of crystalline polymorphs.

In traditional organic film growth RAS can detect thickness changes down to 1/50 of a single molecular layer thickness, *i.e.*, well above the sensitivity of standard monitoring techniques, such as those employing crystal quartz microbalances [8].

Nowadays, an advancement in organic film growth engineering foresees going beyond the simple stacking of molecular units held by Van der Waals interactions, in favour of a more directional type of bonding. Recently, we proposed a new paradigm for the growth of complex molecular films using highly directional coordination bonds. The proposed structure foresees the 1:1 coordination of a Co^{II} tetraphenylporphyrin (CoTPP) and a ditopic linear ligand (N,N'-di(4-pyridyl)-1,4,5,8-naphthalenetetracarboxdiimide, DPNDI), with the latter coordinating the Co metal ion in the free axial position, through one of their pyridyl heads. A sketch of the DPNDI:CoTPP complex is shown in Fig. 1.

The complete film results from the alternated stacking of ordered in-plane arrays of porphyrin (the *floors*) and out-of-plane DPNDI (the *pillars*) molecules, with the first porphyrin layer in contact with the substrate, as described in Ref. [13].

When extending the optical monitoring of organic film growth to these novel films based on metal coordination, we face a critical bottleneck: their structure being highly symmetric, they might produce a rather weak RAS signal. *Pillar* structures, having their polarizable dipole moment along the principal axis, cannot be detected by RAS [14], while for the horizontal *floor*, a possible strategy foresees the use of stepped (vicinal) substrate surfaces [15]. We thus proceed as follows: (i) the first CoTPP layer is grown on an Au(0 0 1) stepped surface, to exploit the ledges and steps to steer the porphyrin assembly. Atomic Force Microscopy (AFM) is employed to check sample morphology of the organic film. (ii) Low Energy Electron Diffraction (LEED), Photoemission Spectroscopy (PES) and Inverse Photoemission Spectroscopy (IPES) techniques are used to assess the differences in the molecular assembly and the electronic properties when the Au(0 0 1) flat surface is replaced by the stepped one. (iii) One of the two polarization directions of the RAS beam (*e.g.,* α) is aligned along the steps, *i.e.,* in the direction of preferential porphyrin assembly.

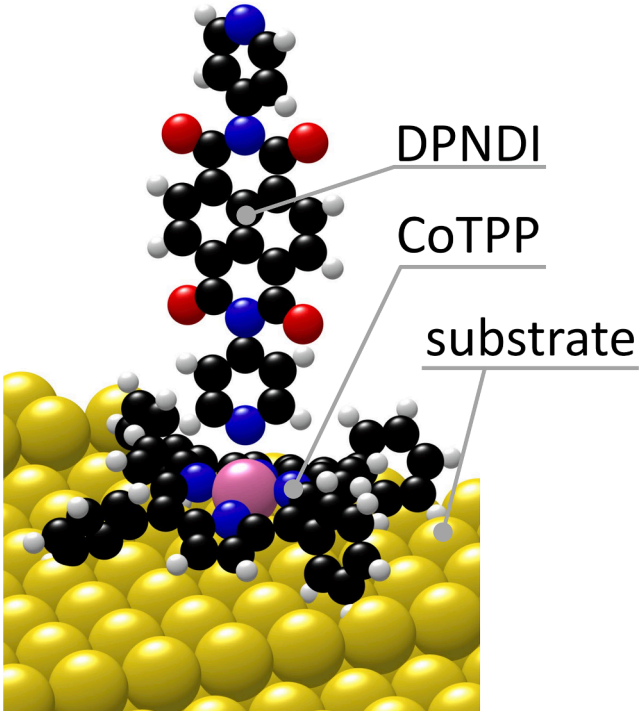

Fig. 1. Schematics of the axially coordinated DPNDI:CoTPP complex. Color code: yellow = gold, pink = cobalt, black = carbon, blue = Nitrogen, red = oxygen, white = hydrogen.

The RAS spectroscopic results, together with a simulation of the absorbance spectrum of DPNDI, as acquired on flat and stepped Au(0 0 1), are then critically reviewed in view of assessing the RAS technique's applicability in the monitoring of axially coordinated molecular films.

2. Methods

2.1. Substrate preparation

We used both flat Au(0 0 1) and vicinal Au(0 0 1) substrates with a cut-off angle of 6° with respect to the [001] direction (purchased from Surface Preparation Laboratory GmbH) for the deposition of molecules. The vicinal tilt axis, *i.e.*, the axis lying in the surface plane about which the sample was rotated out of the low-index orientation before polishing the surface [16], lies along the [1 1 0] direction. Au surfaces were cleaned in ultra-high vacuum (UHV) conditions (base pressure of $6{\cdot}10^{-11}$ Torr) by subjecting them to several alternate cycles of Ar^{+} sputtering (beam energy: 1 keV) and annealing at 400 °C for 20 min by electron bombardment. After the annealing, the cooling down is performed at a slow rate to prevent step-bunching [17]. The good quality of the Au surfaces is confirmed by LEED and PES.

2.2. Molecular films preparation

After their in-vacuum purification, CoTPP (purchased from Merck KGaA) and DPNDI [18] powders were deposited on Au surfaces by molecular beam epitaxy using commercial Kundsen cells equipped with heated quartz crucibles. The evaporation temperatures were 285 °C and 210 °C for CoTPP and DPNDI, respectively, yielding a molecular flux of about 1Å/min, calibrated with a quartz crystal microbalance. The nominal thickness for 1 ML of CoTPP is 3.06 Å [19]. We define 1 ML of DPNDI as the amount of molecules present in 1 ML of CoTPP.

2.3. Spectroscopic techniques

In-situ RAS experiments were performed at room temperature and at near-normal incidence in the ultraviolet–visible (UV–vis) range using a home-made experimental apparatus [20]. The light is produced by a Xe arc lamp and linearly polarized by a Glan polarizer. A photo-elastic modulator (PEM) is then used to modulate the polarization direction (from α to β) at a rate of 100 kHz. The light reflected from the sample passes through a second Glan polarizer and is focused inside a monochromator. The reflectivity anisotropy is directly obtained using a lock-in amplifier, synchronized with the PEM. The experimental geometry is designed to have the linear polarization along the [110] and [$\bar{1}$10] high symmetry directions of the gold substrate. In this way, the α (β) direction is parallel (perpendicular) to the atomic step-edge direction. RAS spectra were collected in the 2 – 3.5 eV photon energy range; however, to focus on the main porphyrin optical transition, only a shorter energy region, centred on the Soret band [8] is discussed in the text.

PES experiments were performed using a He discharge lamp with a photon energy of $h\nu$ = 21.2 eV (the technique is therefore also called ultraviolet photoelectron spectroscopy, UPS). The electron kinetic energy was measured with a 150 mm hemispherical analyser (from SPECS GmbH). The Full Width at Half Maximum (FWHM) energy resolution of PES, with the analyser pass energy fixed at 1 eV, was 15 meV.

IPES experiments were performed to probe the unoccupied electronic levels of CoTPP. In IPES, photons are collected as a result of the radiative de-excitation of electrons impinging on the sample. Low energy electrons are photoemitted from a GaAs crystal, treated with a CsOx layer to obtain the Negative Electron Affinity condition at the surface

(NEA-GaAs), and accelerated on the sample by an electron optics (kinetic energy = 5–16 eV). The emitted photons are measured using a bandpass detector at a fixed energy of 9.6 eV (isochromat mode) yielding a FWHM of 700 meV. The capabilities of the experimental apparatus used to perform photoemission (inverse photoemission) measurements at different electron emission (incidence) angles are better described elsewhere [21,22].

2.4. Structural and morphological techniques

LEED was performed with a commercial apparatus (Physical Electronics Inc.) equipped with a beam shutter. LEED images were taken at an incident beam energy of 55 eV after the spectroscopic characterizations, by exposing the sample to the electron beam for a few seconds.

AFM characterizations were performed by using a commercial scanning probe microscope (5500 by Keysight Technology). The images were acquired in tapping-mode and in attractive regime, with silicon tips from Nanosensors™ (cantilever force constant: 42 N/m; $\nu_0 = 330$ kHz); typical scan rates of about 1 Hz were used. AFM images were also analysed by applying a two-dimensional (2D) autocorrelation function (available in the Gwyddion software) which, line-by-line, describes the interdependence of surface heights, thus highlighting preferential directions and periodicities in the surface texture.

2.5. Computational approach

The optimized geometry of the gas-phase DPNDI molecule was computed using density functional theory (DFT), as implemented in version 5.0 of the ORCA code [23]. Simulations were performed using the B3LYP hybrid exchange–correlation functional [24,25] and the correlation-consistent aug-cc-pVTZ basis set [26].

The theoretical photo-absorption cross section was obtained by means of Green's function-based many-body perturbation theory (MBPT) simulations performed on top of ground-state DFT calculations, using the MOLGW code [27]. This approach offers a valid and accurate alternative to more refined and computationally expensive quantum-chemistry methods for computing excited-state properties of molecular systems [28,29].

Starting with the fully relaxed atomic structure from ORCA, the DFT Kohn–Sham eigenvalues and eigenfunctions are recalculated in a consistent way using the same B3LYP functional and basis set expansion. Electronic energy levels are then obtained within the one-shot perturbative G0W0 approach, and finally the optical spectra, including excitonic effects, are obtained by solving the Bethe Salpeter Equation.

3. Results and discussion

3.1. CoTPP structural and morphological analysis

The typical diffraction pattern of the reconstructed (5 × 20) or hex-Au (0 0 1) [30,31]surface of flat Au(0 0 1) is shown in Fig. 2a (see Ref. [32] and references therein for a more detailed analysis of the observed pattern). At 1 ML coverage, CoTPP molecules form an ordered (5 × 5) superstructure that is commensurate with the underlying Au(0 0 1) surface. Such a (5 × 5) symmetry was previously observed in the case of ZnTPP on Au(0 0 1) and Fe-p(1 × 1)O [31].

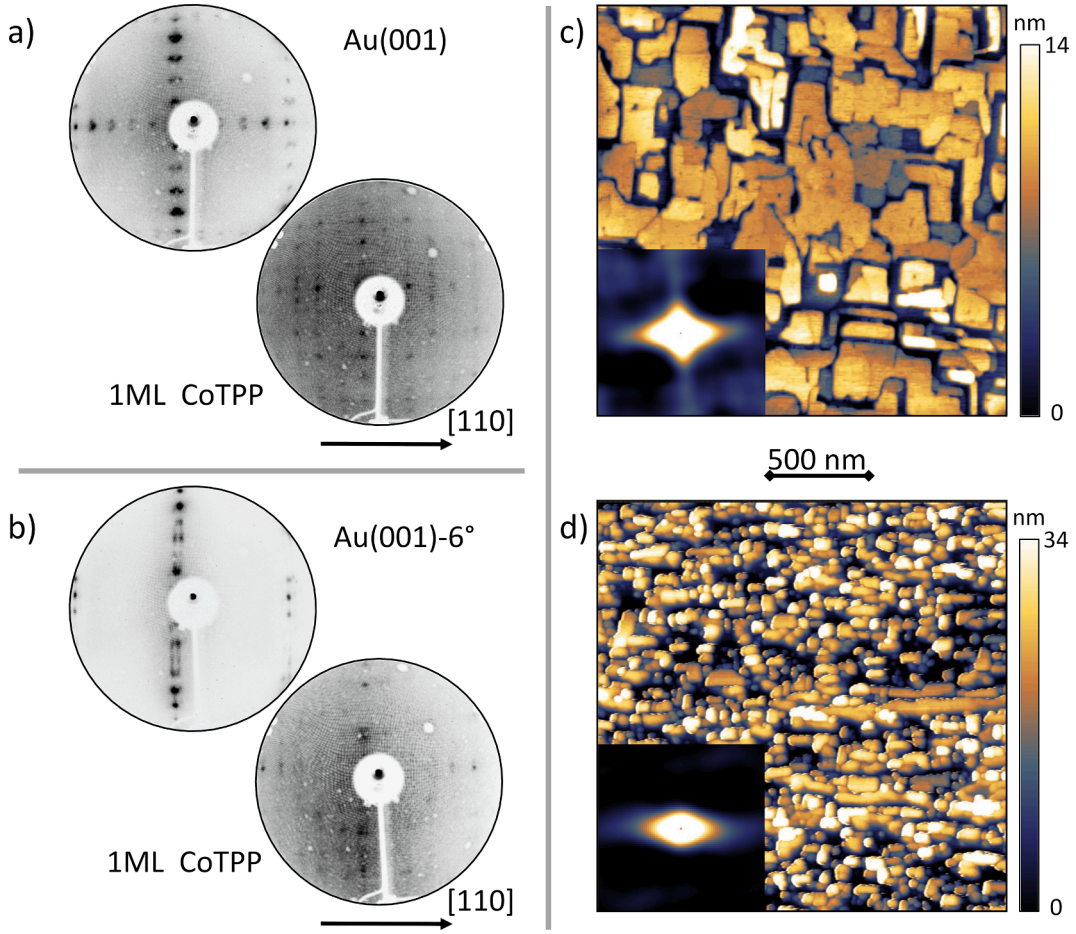

Fig. 2. LEED patterns acquired at 55 eV for the bare substrate and 1 ML of CoTPP on a) flat Au(0 0 1) and b) vicinal Au(0 0 1)-6°. AFM images acquired for 16 ML of CoTPP on c) flat Au(0 0 1) and d) vicinal Au(0 0 1)-6°. Insets (c, d): 2D autocorrelation function of the AFM images. The crystallographic directions are the same for both LEED and AFM. Step edges lie in the [1 1 0] direction.

The LEED pattern of vicinal Au(001)-6° is shown in Fig. 2b. The extra spots associated to the surface reconstruction are present only in the direction perpendicular to [110]. This is due to the presence of monoatomic steps (theoretical step width: about 1.5 nm), forcing the alignment of the hex-Au close packed atomic rows [33] only along the step direction, as observed on vicinal-Au(001) surfaces for different cut-off angles [16]. When 1 ML of CoTPP molecules is deposited on this vicinal surface, a LEED pattern compatible with the one observed on flat Au(001) appears. For thicker CoTPP layers, the LEED pattern disappears, while when 1 ML DPNDI is deposited onto 1 ML CoTPP, the diffraction pattern is preserved (Figure S1 of the Supplementary Information).

For a thicker CoTPP film (16 ML) deposited on flat and vicinal Au (001)-6°, *ex-situ* AFM images were acquired (Fig. 2c and d, respectively). CoTPP crystals show different lateral sizes when the growth takes place on the two different surfaces. The role of steps in triggering a preferential growth direction can be best appreciated by inspection of the inset figures, where a 2D autocorrelation function is applied to the morphological image. On flat-Au(001), CoTPP molecules form large and flat structures with sharp edges extending along the [110] and [$\bar{1}$10] directions with equal probability. The overall behaviour of the molecules is drastically changed in the case of CoTPP on vicinal Au(001)-6°. Molecular structures with sharp edges are still present, but there is clear evidence of a preferential direction for their growth and a reduction in the average size of the structures. As also shown by the 2D autocorrelation function, the symmetry of the system is no longer maintained. There is, therefore, an important difference in the growth of molecules, with crystal edges preferentially elongated towards the step direction.

3.2. CoTPP electronic analysis

To avoid strong interactions between the first molecular layer deposited on the substrate and the substrate itself, the authors have already proved the key role of surface passivation before molecular deposition [31] However, considering the intrinsic variability characteristic of the passivation layers stabilized on vicinal surfaces with respect to their flat counterparts [34], we decided to revert to a less reactive substrate such as Au(001), on which ordered porphyrin layers can be stabilized (see previous section). The results of our photoemission characterization are shown in Fig. 3. The PES (IPES) spectra were acquired by detecting (sending) electrons in the [001] direction, *i.e.*, perpendicular to the steps' surface.

The spectra acquired on a 16 ML thick sample (green) are representative of CoTPP molecules not interacting with the substrate [31] and are here used just to identify the CoTPP features. Dotted lines highlight a shift of such features towards the Fermi energy (E_F) going from the multilayer to the 1 ML CoTPP samples (shown as blue and red spectra in Fig. 3), which is due to the larger screening of the photogenerated hole (added electron) by the substrate in PES (IPES), as reported in Ref. [19]. On both Au(001) and vicinal Au(001)-6°, the Highest Occupied Molecular Orbital (HOMO) and the Lowest Unoccupied Molecular Orbital (LUMO) levels are clearly identified. This is a crucial condition to ensure the electronic stability of the deposited molecules while in contact with the substrate and a prerequisite for the axial coordination with DPNDI molecules. The black arrow identifies a feature related to the presence of an interface state [35,36].

On the 1 ML CoTPP spectra, the remaining features are attributed to photoemission from the Au substrate. However, scattering from the molecular layer itself can alter the lineshape contribution from the underlying substrate, and hence the bare Au(001) and vicinal Au(001)-6° substrate lineshapes (shown as black and yellow spectra in Fig. 3, respectively). Therefore, for a correct interpretation of the 1 ML CoTPP spectra, a better choice is to refer to the photoemission lineshape acquired from a polycrystalline Au reference (turquoise spectrum in Fig. 3, see [37] for further details).

The full angular-resolved photoemission analysis of the above samples, to unveil the possible influence of steps in the electronic structure of the system, is reported in Figure S2 of the Supplementary Information.

3.3. CoTPP optical analysis

The RAS analysis as a function of the deposited molecular thickness shows differences between the two substrates. On the flat Au(001) substrate (Fig. 4a), the RAS signal is characterized by an almost null intensity upon the deposition of the first CoTPP layers. Such a RAS signal can be attributed to an isotropic (5 × 5) arrangement of the molecules, which also show two equivalent polarizable dipole moments [38,39].

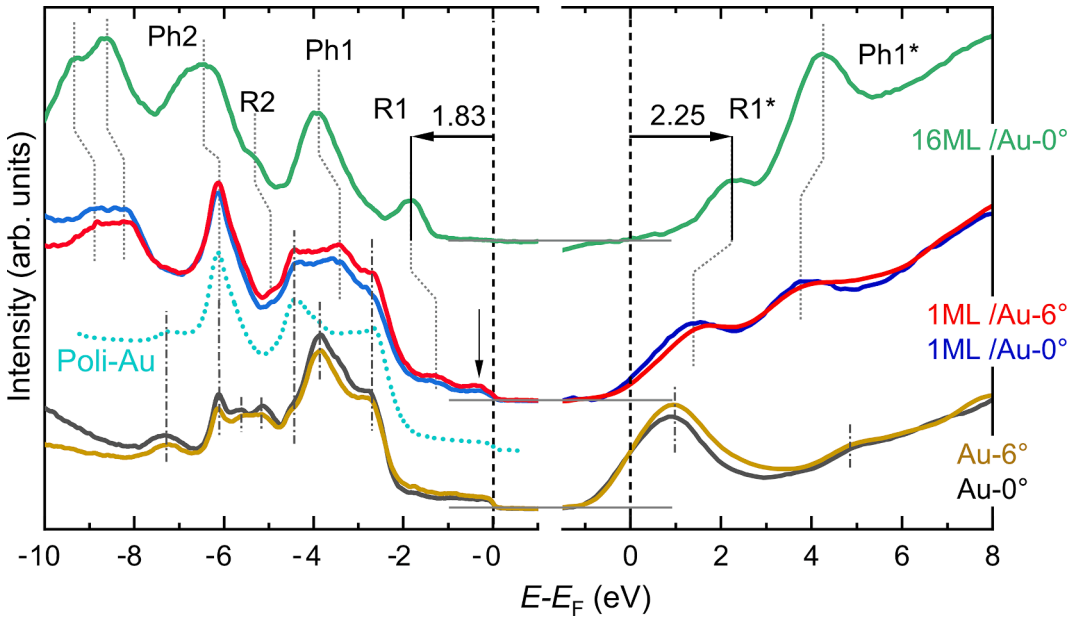

Fig. 3. Normal emission UPS and normal incidence IPES spectra for 16 ML CoTPP, 1 ML CoTPP and the substrates. Both the flat and the vicinal Au sample spectra are shown. The spectrum of polycrystalline Au, shown in turquoise, is adapted from Ref. [37]. The spectroscopic contributions from phenyls (Ph) and the tetrapyrrole ring (R) of the porphyrin molecules are labelled in the image as per Ref. [48].

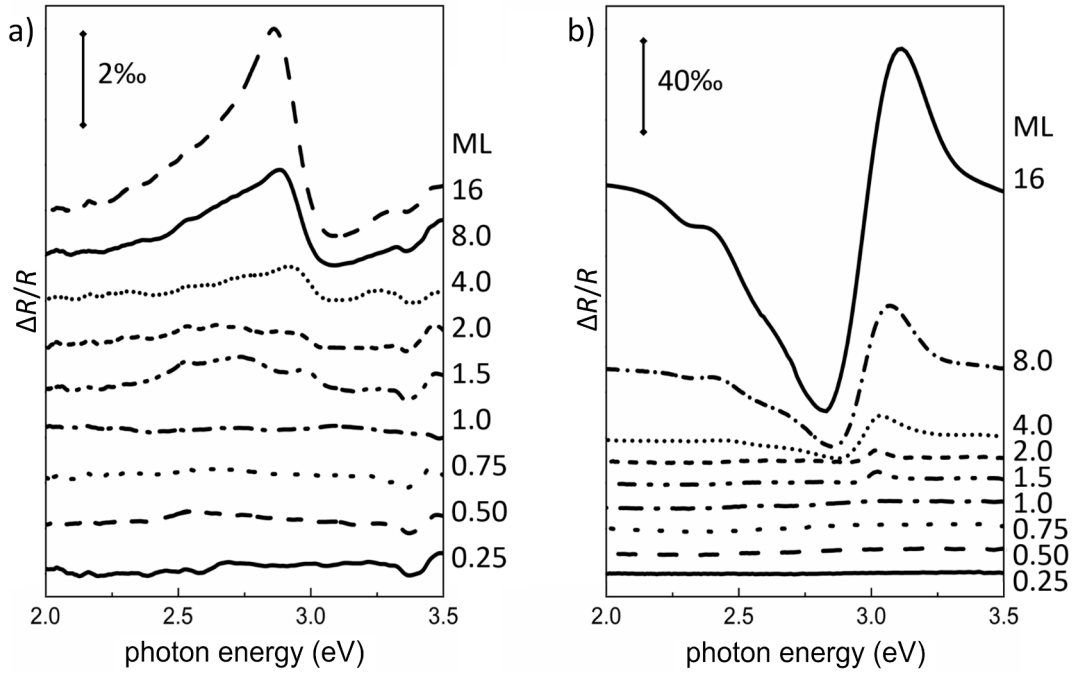

Fig. 4. Incremental RAS spectra acquired during the growth of CoTPP on a) flat Au(001) and b) vicinal Au(001)-6°.

Above 4 ML [40], the molecular packing (molecule tilt angle) changes. Consequently, the equivalence between the polarizable dipole moments is broken, as described by Mendoza *et al.* [41], and a non-zero RAS signal is detected (≈4‰). The peak anisotropy is detected at about 2.9 eV, where the main Soret band is placed. It is interesting to compare this result with the HOMO-LUMO gap evaluated by measuring the energy difference between the R1 and R1* peaks on the 16 ML CoTPP sample (Fig. 3). The UPS-IPES energy gap $\left(E_{gap}^{UPS-IPES}\right)$ is 4.1 eV, about 1.2 eV larger than the optical gap $\left(E_{gap}^{RAS}\right)$, obtained from the energy position of the Soret band. This energy difference, corresponding to the binding energy of the Frenkel exciton ($E_{exc} = E_{gap}^{UPS\text{-}IPES} - E_{gap}^{RAS} \approx 1.2$ eV), falls within the expected range for TPP molecules [42–45].

On the vicinal Au(001) substrate (Fig. 4b), the RAS signal obtained for the incremental deposition of CoTPP is significantly different from the one observed on the flat Au(001) sample; in particular, a RAS anisotropy up to 150‰ is observed on the thickest CoTPP film. The RAS signal enhancement agrees with our morphological characterization (see previous section). We note that, instead of observing a peak-like feature as in panel a), the RAS spectrum is characterized by a "derivative-like" lineshape, also reported by Goletti *et al.* [46] which precludes the possibility of a direct interpretation of the sign of the RAS signal and the correct determination of the film main adsorbance peak [46]. As commented by Castillo *et al.* [14], this effect is related to a larger degree of order of the polarizable dipole moments, also in the direction of light propagation, *i.e.,* perpendicular to the surface. This might imply that the presence of smaller and highly oriented crystals fostered by the presence of steps might also influence the out of plane stacking of the molecules.

The role of vicinal surfaces in triggering a RAS signal is also visible on the CoTPP single layer. In Fig. 5, on flat Au(001), experimental data points are scattered on a mean value that is close to zero (horizontal dotted line). Conversely, the signal from 1 ML CoTPP on vicinal Au (001)-6° is close to 1‰ and is positive, implying a preferential alignment of the polarizable dipole moment along the steps direction.

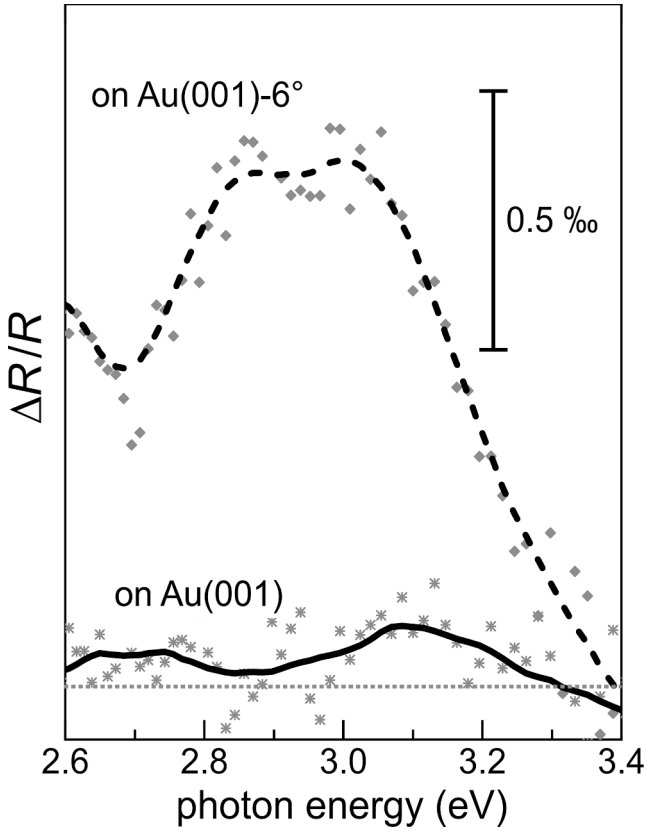

Fig. 5. RAS signals for 1 ML CoTPP on Au(001) and Au(001)-6°.

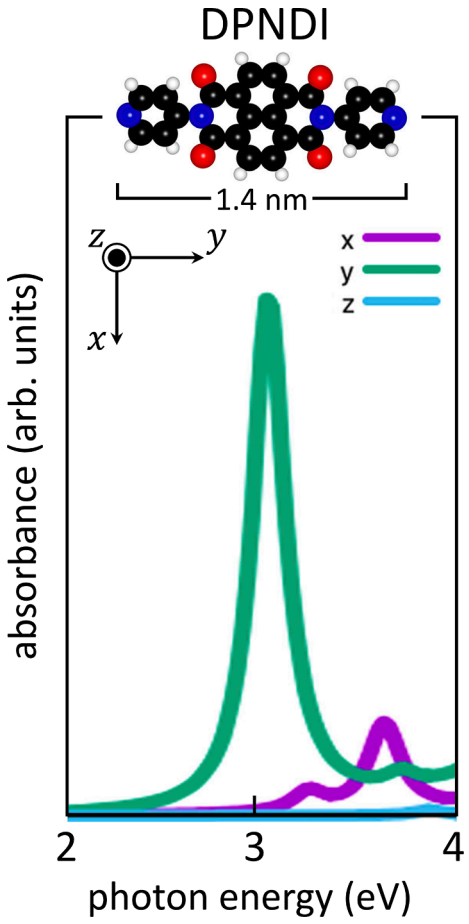

Fig. 6. Calculated absorbance for the free DPNDI molecule.

3.4. DPNDI-CoTPP axial coordination monitored by RAS

A preliminary investigation of the optical properties of DPNDI molecules before their deposition on top of CoTPP is mandatory. In Fig. 6, we report the calculated absorbance properties of the DPNDI molecule for light polarized along different symmetry directions. The main effect is observed when the electric field is aligned along the main molecular axis (*y* direction). Since DPNDI molecules, similar to CoTPP, tend to lie flat on the substrate at submonolayer coverages [13], we deposited 1 ML DPNDI on vicinal Au(0 0 1)-6° to enhance their optical response. Indeed, the related RAS spectrum (Fig. 7, bottom spectrum) shows a peak centred at 3.1 eV, in close agreement with the theoretical prediction. In the same image, we report, for clarity, the spectrum of 1 ML CoTPP on vicinal Au(0 0 1)-6°. Subsequently, 1 ML of DPNDI was coordinated on top of this CoTPP layer. The RAS spectrum of the DPNDI:CoTPP complex is reported in Fig. 7, top spectrum. In this case, no additional shoulder is observed at the photon energy characteristic of DPNDI absorption. In addition, the overall signal anisotropy is comparable with that of the CoTPP layer underneath. We only observe a slight red shift of the CoTPP feature by about 100 meV, that represents the changes occurring in the Soret band position when porphyrin molecules interact with analytes [47]. The evolution of the data collected from the CoTPP layer and from the DPNDI:CoTPP complex is thus compatible with (i) the polarizable dipole moments expected from both molecular species; (ii) the axial coordination of these molecules; (iii) the interaction between the pyridyl head of DPNDI and the porphyrin central metal ion.

In the Supplementary Information, we present a schematic diagram (Figure S3) showing a molecular arrangement for DPNDI, CoTPP and the DPNDI:CoTPP complex on vicinal Au(0 0 1)-6°, compatible with the presented experimental results.

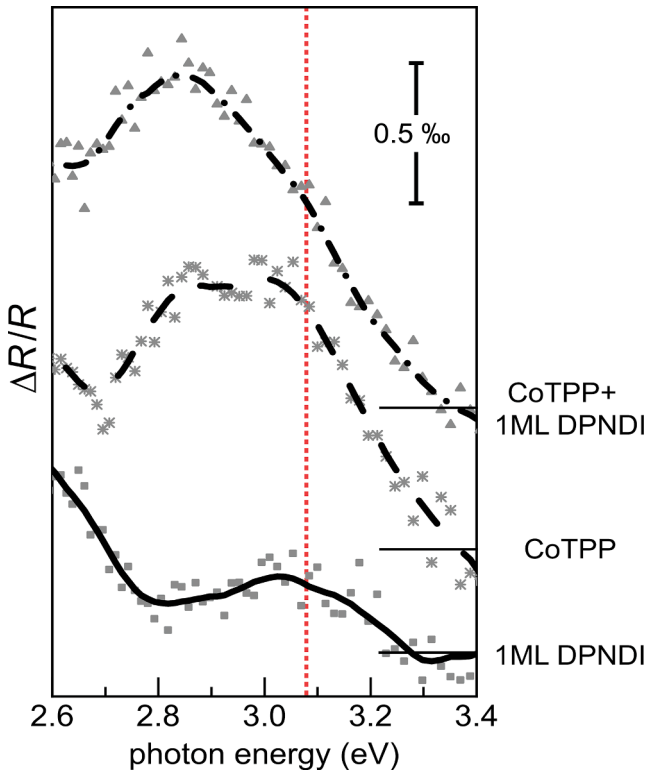

Fig. 7. From bottom to top: RAS spectra acquired on 1ML DPNDI, 1 ML CoTPP and the DPNDI:CoTPP axial complex, all grown on vicinal Au(0 0 1)-6°. The red line at a photon energy of 3.1 eV marks the position of peak DPNDI optical absorption.

4. Conclusions

RAS is a consolidated technique to monitor the growth of organic films, where the multilayer growth is driven by Van der Waals interactions. In such systems, a direct correspondence can be established between the intensity of the RAS signal and the thickness of the molecular film. Recently, we proposed a new paradigm in organic film growth where molecule:molecule complexes are fabricated by the sequential deposition of the constituent compounds. In these films, molecules interact via coordination chemistry. A prototype system of such a novel film growth is provided by the DPNDI:CoTPP complex, characterized by the axial coordination of the porphyrin central metal atom with one of the pyridyl heads of DPNDI ligand. The assembled film structure is highly symmetric, possibly resulting in a hardly detectable RAS signal.

Clearly, based on this premise, a different approach in film growth monitoring is required. We induced an optical anisotropy in the CoTPP film by ordered deposition on an atomically stepped Au vicinal substrate. We successfully observed a clear RAS signal on the CoTPP film, while, upon the addition of axially coordinated DPNDI molecules, we certify that the RAS signal (within 0.1‰) retains the same intensity and lineshape of CoTPP in the spectral region characterized by DPNDI optical absorption. As a consequence of this study, we conclude that the range of applicability of RAS can indeed be extended to axially coordinated compounds, with the additional requirement of a more accurate analysis of the spectra, considering the precise lineshape, instead of just the intensity evolution.

CRediT authorship contribution statement

F. Goto: Investigation, Data curation, Writing – original draft. **A. Calloni:** Conceptualization, Supervision, Writing – review & editing. **I.**

Majumdar: Investigation, Writing – review & editing. **R. Yivlialin:** Investigation, Formal analysis. **C. Filoni:** Investigation. **C. Hogan:** Investigation, Software, Formal analysis. **M. Palummo:** Investigation, Formal analysis. **A. Orbelli Biroli:** Resources, Validation. **M. Finazzi:** Validation, Writing – review & editing. **L. Duò:** Resources, Writing – review & editing. **F. Ciccacci:** Funding acquisition, Writing – review & editing. **G. Bussetti:** Conceptualization, Supervision, Project administration, Writing – review & editing.

Declaration of Competing Interest

The authors declare that they have no known competing financial interests or personal relationships that could have appeared to influence the work reported in this paper.

Data availability

Data will be made available on request.

Acknowledgements

IM acknowledges the financial support from the Marie Skłodowska-Curie Action (MSCA) Seal of Excellence Individual Fellowship 2020 under grant n° UA.A.RRR.DFIS.PAMM.STUD.BGP1VARI01. AOB acknowledges support from the Ministero dell'Università e della Ricerca (MUR) and the University of Pavia through the program "Dipartimenti di Eccellenza 2023–2027".

The authors would like to thank G. Albani and L. Ferraro (Politecnico di Milano), A. Bossi (Istituto di Scienze e Tecnologie Chimiche "G. Natta", CNR-SCITEC), L. Floreano (IOM-CNR) and L. Schio (Elettra Synchrotron) for fruitful discussions.

Appendix A. Supplementary data

Supplementary data to this article can be found online at https://doi.org/10.1016/j.ica.2023.121612.

References

[1] L.L. Li, E.W.G. Diau, Porphyrin-sensitized solar cells, Chem. Soc. Rev. 42 (1) (2013) 291–304, https://doi.org/10.1039/c2cs35257e.
[2] J. Min Park, J.H. Lee, W.-D. Jang, Applications of porphyrins in emerging energy conversion technologies, Coord. Chem. Rev. 407 (2020) 213157, https://doi.org/10.1016/j.ccr.2019.213157.
[3] M. Jurow, A.E. Schuckman, J.D. Batteas, C.M. Drain, Porphyrins as molecular electronic components of functional devices, Coord. Chem. Rev. 254 (19–20) (2010) 2297–2310, https://doi.org/10.1016/j.ccr.2010.05.014.
[4] R. Paolesse, S. Nardis, D. Monti, M. Stefanelli, C. Di Natale, Porphyrinoids for Chemical Sensor Applications, Chem. Rev. 117 (4) (2017) 2517–2583, https://doi.org/10.1021/acs.chemrev.6b00361.
[5] G. Bussetti, C. Corradini, C. Goletti, P. Chiaradia, M. Russo, R. Paolesse, C. Di Natale, A. D'Amico, L. Valli, Optical anisotropy and gas sensing properties of ordered porphyrin films, Phys. Status Solidi B Basic Res. 242 (13) (2005) 2714–2719, https://doi.org/10.1002/pssb.200541104.
[6] G. Di Carlo, A.O. Biroli, F. Tessore, S. Caramori, M. Pizzotti, β-Substituted ZnII porphyrins as dyes for DSSC: A possible approach to photovoltaic windows, Coord. Chem. Rev. 358 (2018) 153–177, https://doi.org/10.1016/j.ccr.2017.12.012.
[7] M. Urbani, M. Grätzel, M.K. Nazeeruddin, T. Torres, Meso-Substituted Porphyrins for Dye-Sensitized Solar Cells, Chem. Rev. 114 (24) (2014) 12330–12396, https://doi.org/10.1021/cr5001964.
[8] C. Goletti, G. Bussetti, P. Chiaradia, A. Sassella, A. Borghesi, The application of reflectance anisotropy spectroscopy to organics deposition, Org. Electron. 5 (1–3) (2004) 73–81, https://doi.org/10.1016/j.orgel.2004.01.002.
[9] S.R. Forrest, Ultrathin Organic Films Grown by Organic Molecular Beam Deposition and Related Techniques, Chem. Rev. 97 (1997) 1793–1896, https://doi.org/10.1021/cr941014o.
[10] H. Proehl, R. Nitsche, T. Dienel, K. Leo, T. Fritz, In situ differential reflectance spectroscopy of thin crystalline films of PTCDA on different substrates, Phys. Rev. B 71 (16) (2005) 165207, https://doi.org/10.1103/PhysRevB.71.165207.
[11] D.S. Martin, P. Weightman, Reflection anisotropy spectroscopy: A new probe of metal surfaces, Surf. Interface Anal. 31 (10) (2001) 915–926, https://doi.org/10.1002/sia.1129.
[12] P. Weightman, D.S. Martin, R.J. Cole, T. Farrell, Reflection anisotropy spectroscopy, Rep. Prog. Phys. 68 (6) (2005) 1251–1341, https://doi.org/10.1088/0034-4885/68/6/R01.
[13] A. Orbelli Biroli, A. Calloni, A. Bossi, M.S. Jagadeesh, G. Albani, L. Duò, F. Ciccacci, A. Goldoni, A. Verdini, L. Schio, L. Floreano, G. Bussetti, Out-Of-Plane Metal Coordination for a True Solvent-Free Building with Molecular Bricks: Dodging the Surface Ligand Effect for On-Surface Vacuum Self-Assembly, Adv. Funct. Mater. 31 (20) (2021), 2011008, https://doi.org/10.1002/adfm.202011008.
[14] C. Castillo, R.A. Vazquez-Nava, B.S. Mendoza, Reflectance anisotropy for porphyrin octaester Langmuir-Schaefer films, Physica Status Solidi C: Conferences (2003) 2971–2975, https://doi.org/10.1002/pssc.200303859.
[15] S. Boudet, I. Bidermane, E. Lacaze, B. Gallas, M. Bouvet, J. Brunet, A. Pauly, Y. Borensztein, N. Witkowski, Growth mode and self-organization of $LuPc_2$ on Si (001)-2×1 vicinal surfaces: An optical investigation, Phys. Rev. B: Condens. Matter Mater. Phys. 86 (11) (2012) 115413, https://doi.org/10.1103/PhysRevB.86.115413.
[16] M. Rickart, T. Mewes, S.O. Demokritov, B. Hillebrands, M. Scheib, Correlation between topography and magnetic surface anisotropy in epitaxial Fe films on vicinal-to-(001) Au surfaces with different step orientation, Phys. Rev. B: Condens. Matter Mater. Phys. 70 (6) (2004), 060408, https://doi.org/10.1103/PhysRevB.70.060408.
[17] N. Néel, J. Kröger, R. Berndt, Fullerene nanowires on a vicinal gold surface, Appl. Phys. Lett. 88 (16) (2006) 163101, https://doi.org/10.1063/1.2195530.
[18] D.R. Trivedi, Y. Fujiki, Y. Goto, N. Fujita, S. Shinkai, K. Sada, A naked-eye colorimetric indicator to discriminate aromatic compounds by solid-state charge-transfer complexation, Chem. Lett. 37 (5) (2008) 550–551, https://doi.org/10.1246/cl.2008.550.
[19] A. Calloni, M.S. Jagadeesh, G. Bussetti, G. Fratesi, S. Achilli, A. Picone, A. Lodesani, A. Brambilla, C. Goletti, F. Ciccacci, L. Duò, M. Finazzi, A. Goldoni, A. Verdini, L. Floreano, Cobalt atoms drive the anchoring of Co-TPP molecules to the oxygen-passivated Fe(0 0 1) surface, Appl. Surf. Sci. 505 (2020), 144213, https://doi.org/10.1016/j.apsusc.2019.144213.
[20] G. Bussetti, L. Ferraro, A. Bossi, M. Campione, L. Duò, F. Ciccacci, A microprocessor-aided platform enabling surface differential reflectivity and reflectance anisotropy spectroscopy, Eur. Phys. J. Plus 136 (4) (2021) 421, https://doi.org/10.1140/epjp/s13360-021-01346-7.
[21] F. Goto, A. Calloni, G. Albani, A. Picone, A. Brambilla, C. Zucchetti, F. Bottegoni, M. Finazzi, L. Duò, F. Ciccacci, G. Bussetti, Mapping the evolution of Bi/Ge(111) empty states: From the wetting layer to pseudo-cubic islands, J. Appl. Phys. 129 (15) (2021) 155310, https://doi.org/10.1063/5.0048275.
[22] G. Berti, A. Calloni, A. Brambilla, G. Bussetti, L. Duò, F. Ciccacci, Direct observation of spin-resolved full and empty electron states in ferromagnetic surfaces, Rev. Sci. Instrum. 85 (7) (2014), 073901, https://doi.org/10.1063/1.4885447.
[23] F. Neese, Software update: The ORCA program system—Version 5.0, WIREs Comput. Mol. Sci. 12 (5) (2022) 1606, https://doi.org/10.1002/wcms.1606.
[24] P.J. Stephens, F.J. Devlin, C.F. Chabalowski, M.J. Frisch, Ab Initio Calculation of Vibrational Absorption and Circular Dichroism Spectra Using Density Functional Force Fields, J. Phys. Chem. 98 (45) (1994) 11623–11627, https://doi.org/10.1021/j100096a001.
[25] A.D. Becke, Density-functional thermochemistry. III. The role of exact exchange, J. Chem. Phys. 98 (7) (1993) 5648–5652, https://doi.org/10.1063/1.464913.
[26] T.H. Dunning, Gaussian basis sets for use in correlated molecular calculations. I. The atoms boron through neon and hydrogen, J. Chem. Phys. 90 (2) (Jan. 1989) 1007–1023, https://doi.org/10.1063/1.456153.
[27] F. Bruneval, T. Rangel, S.M. Hamed, M. Shao, C. Yang, J.B. Neaton, molgw 1: Many-body perturbation theory software for atoms, molecules, and clusters, Comput. Phys. Commun. 208 (2016) 149–161, https://doi.org/10.1016/j.cpc.2016.06.019.
[28] X. Blase, I. Duchemin, D. Jacquemin, The Bethe-Salpeter equation in chemistry: relations with TD-DFT, applications and challenges, Chem. Soc. Rev. 47 (3) (2018) 1022–1043, https://doi.org/10.1039/C7CS00049A.
[29] X. Blase, I. Duchemin, D. Jacquemin, P.-F. Loos, The Bethe-Salpeter Equation Formalism: From Physics to Chemistry, J. Phys. Chem. Lett. 11 (17) (2020) 7371–7382, https://doi.org/10.1021/acs.jpclett.0c01875.
[30] Y. Jiang, X. Liang, S. Ren, C.-L. Chen, L.-J. Fan, Y.-W. Yang, J.-M. Tang, D.-A. Luh, The growth of sulfur adlayers on Au(100), J. Chem. Phys. 142 (6) (2015), 064708, https://doi.org/10.1063/1.4907789.
[31] G. Bussetti, A. Calloni, M. Celeri, R. Yivlialin, M. Finazzi, F. Bottegoni, L. Duò, F. Ciccacci, Structure and electronic properties of Zn-tetra-phenyl-porphyrin single- and multi-layers films grown on Fe(001)-p(1 × 1)O, Appl. Surf. Sci. 390 (2016) 856–862, https://doi.org/10.1016/j.apsusc.2016.08.137.
[32] R. Hammer, A. Sander, S. Förster, M. Kiel, K. Meinel, W. Widdra, Surface reconstruction of Au(001): High-resolution real-space and reciprocal-space inspection, Phys. Rev. B 90 (3) (2014), 035446, https://doi.org/10.1103/PhysRevB.90.035446.
[33] S. Bengió, V. Navarro, M.A. González-Barrio, R. Cortés, I. Vobornik, E.G. Michel, A. Mascaraque, Electronic structure of reconstructed Au(100): Two-dimensional and one-dimensional surface states, Phys. Rev. B 86 (4) (2012), 045426, https://doi.org/10.1103/PhysRevB.86.045426.
[34] C. Tegenkamp, Vicinal surfaces for functional nanostructures, J. Phys. Condens. Matter 21 (1) (2009) 013002, https://doi.org/10.1088/0953-8984/21/1/013002.
[35] W. Hieringer, K. Flechtner, A. Kretschmann, K. Seufert, W. Auwärter, J.V. Barth, A. Görling, H.-P. Steinrück, J.M. Gottfried, The surface trans effect: Influence of axial ligands on the surface chemical bonds of adsorbed metalloporphyrins, J. Am. Chem. Soc. 133 (16) (2011) 6206–6222, https://doi.org/10.1021/ja1093502.

[36] Y. Bai, M. Sekita, M. Schmid, T. Bischof, H.-P. Steinruk, J. Michael Gottfried, Interfacial coordination interactions studied on cobalt octaethylporphyrinand cobalt tetraphenylporphyrin monolayers on Au(111), PCCP 12 (17) (2010) 4273–4274, https://doi.org/10.1039/c004746p.

[37] L. Giovanelli, F.C. Bocquet, P. Amsalem, H.-L. Lee, M. Abel, S. Clair, M. Koudia, T. Faury, L. Petaccia, D. Topwal, E. Salomon, T. Angot, A.A. Cafolla, N. Koch, L. Porte, A. Goldoni, J.-M. Themlin, Interpretation of valence band photoemission spectra at organic-metal interfaces, Phys. Rev. B: Condens. Matter Mater. Phys. 87 (3) (2013), 035413, https://doi.org/10.1103/PhysRevB.87.035413.

[38] G. Bussetti, M. Campione, A. Sassella, L. Duò, Optical and morphological properties of ultra-thin H_2TPP, H_4TPP and ZnTPP films, Phys Status Solidi B Basic Res 252 (1) (2015) 100–104, https://doi.org/10.1002/pssb.201350260.

[39] N. Arzate, B.S. Mendoza, R.A. Vázquez-Nava, Polarizable dipole models for reflectance anisotropy spectroscopy: a review, J. Phys.Condensed Matter 16 (39) (2004) S4259–S4278, https://doi.org/10.1088/0953-8984/16/39/002.

[40] A. Picone, D. Giannotti, A. Brambilla, G. Bussetti, A. Calloni, R. Yivlialin, M. Finazzi, L. Duò, F. Ciccacci, A. Goldoni, A. Verdini, L. Floreano, Local structure and morphological evolution of ZnTPP molecules grown on Fe(001)-p(1 × 1)O studied by STM and NEXAFS, Appl. Surf. Sci. 435 (2018) 841–847, https://doi.org/10.1016/j.apsusc.2017.11.128.

[41] B.S. Mendoza, R.A. Vázquez-Nava, Model for reflectance anisotropy spectra of molecular layered systems, Phys. Rev. B: Condens. Matter Mater. Phys. 72 (3) (2005), 035411, https://doi.org/10.1103/PhysRevB.72.035411.

[42] I.G. Hill, A. Kahn, Combined photoemission/in vacuo transport study of the indium tin oxide/copper phthalocyanine/N, N′-diphenyl-N, N′-bis(l-naphthyl)-1,1′biphenyl-4, 4″diamine molecular organic semiconductor system, J. Appl. Phys. 86 (4) (1999) 2116–2122, https://doi.org/10.1063/1.371018.

[43] J. Hwang, A. Wan, A. Kahn, Energetics of metal-organic interfaces: New experiments and assessment of the field, Mater. Sci. Eng. R. Rep. 64 (1–2) (2009) 1–31, https://doi.org/10.1016/j.mser.2008.12.001.

[44] I.G. Hill, A. Kahn, Z.G. Soos, R.A. Pascal, Charge-separation energy in films of p-conjugated organic molecules, Chem. Phys. Lett. 327 (3–4) (2000) 181–188, https://doi.org/10.1016/S0009-2614(00)00882-4.

[45] S. Coh, Electronic structure and binding geometry of tetraphenylporphyrin-derived molecules adsorbed on metal and metal oxide surfaces, Rutgers, The State University of New Jersey (2012), https://doi.org/10.7282/T3NC5ZZT.

[46] C. Goletti, R. Paolesse, E. Dalcanale, T. Berzina, C. Di Natale, G. Bussetti, P. Chiaradia, A. Froiio, L. Cristofolini, M. Costa, A. D'Amico, Thickness dependence of the optical anisotropy for porphyrin octaester Langmuir-Schaefer films, Langmuir 18 (18) (2002) 6881–6886, https://doi.org/10.1021/la025756l.

[47] G. Bussetti, A. Violante, R. Yivlialin, S. Cirilli, B. Bonanni, P. Chiaradia, C. Goletti, L. Tortora, R. Paolesse, E. Martinelli, A. D'Amico, C. Di Natale, G. Giancane, L. Valli, Site-sensitive gas sensing and analyte discrimination in langmuir-blodgett porphyrin films, J. Phys. Chem. C 115 (16) (2011) 8189–8194, https://doi.org/10.1021/jp200303t.

[48] G. Albani, L. Schio, F. Goto, A. Calloni, A. Orbelli Biroli, A. Bossi, F. Melone, S. Achilli, G. Fratesi, C. Zucchetti, L. Floreano, G. Bussetti, Ordered assembly of non-planar vanadyl-tetraphenylporphyrins on ultra-thin iron oxide, PCCP 24 (28) (2022) 17077–17087, https://doi.org/10.1039/D1CP05914A.